Type 3 Secretion Translocators Spontaneously Assemble a Hexadecameric Transmembrane Complex*

Fabian B. Romano[‡1], **Yuzhou Tang**[‡], **Kyle C. Rossi**[§], **Kathryn R. Monopoli**[‡], **Jennifer L. Ross**[‡¶], **and Alejandro P. Heuck**[‡§2]

From the ‡Program in Molecular and Cellular Biology, and the Departments of §Biochemistry and Molecular Biology and ¶Physics, University of Massachusetts, Amherst, Massachusetts 01003

A type 3 secretion system is used by many bacterial pathogens to inject proteins into eukaryotic cells. Pathogens insert a translocon complex into the target eukaryotic membrane by secreting two proteins known as translocators. How these translocators form a translocon in the lipid bilayer and why both proteins are required remains elusive. *Pseudomonas aeruginosa* translocators PopB and PopD insert pores into membranes forming homo- or hetero-complexes of undetermined stoichiometry. Single-molecule fluorescence photobleaching experiments revealed that PopD formed mostly hexameric structures in membranes, whereas PopB displayed a bi-modal distribution with 6 and 12 subunits peaks. However, individually the proteins are not functional for effector translocation. We have found that when added together, the translocators formed distinct hetero-complexes containing 8 PopB and 8 PopD molecules. Thus, the interaction between PopB and PopD guide the assembly of a unique hetero-oligomer in membranes.

The transport of proteins across membranes is essential at many stages of pathogen infection and colonization of human cells. This process typically involves the discharge of proteins from the pathogen (secretion) and the introduction of these secreted toxins/effectors into the cytosol of the target cell (translocation). Many pathogens, including the *Shigella*, *Salmonella*, *Yersinia*, and *Pseudomonas* species, exploit a sophisticated and efficient mechanism of protein secretion and translocation known as type III secretion (T3S)[3] system (1, 2). The T3S system is a syringe-like macromolecular machine formed by more than 20 different proteins organized in three major structures to span: (i) the inner bacterial membrane, the periplasmic space, and the outer bacterial membrane (the

secreton); (ii) the extracellular space (the needle); and (iii) the host cellular membrane (the translocon) (3–6).

A phylogenetic analysis of bacterial T3S systems based on conservation of their basal body ATPase indicates the presence of at least 7 families of T3S machines. The *Pseudomonas aeruginosa* genome encodes a single T3S system grouped within the Ysc family, named after the *Yersinia* spp. T3S system (the archetypical T3S system in this family) (7). The Ysc family includes pathogens like *Yersinia pestis*, *Y. pseudotuberculosis*, *Y. enterocolitica*, *Bordetella pertussis*, *Vibrio parahemeolyticus*, and *P. aeruginosa*, among others. The Ysc family shares structural similarity with the Inv-Mxi-Spa family of T3S systems, which includes the secretion systems used by *Salmonella enterica* and *Shigella* spp. (8).

Great progress has been made in the structural characterization of the secreton and the needle for different T3S system families (9). However, little is known about how T3S-secreted proteins are translocated across the plasma membrane of the target cell to alter the normal function of the host (4). Two T3S-secreted proteins, known as the T3S translocators, insert into the target membrane to facilitate effector translocation. *P. aeruginosa* translocators PopB/PopD and the tip forming protein PcrV are functionally conserved with the *Yersinia* homologues YopB/YopD and LcrV, suggesting a common translocation mechanism. Placing PopB and PopD in a YopB/YopD-deficient *Y. pseudotuberculosis* strain rescues full translocation of T3S effectors into HeLa cells as well as a T3S-dependent pore-forming phenotype in erythrocytes, if PcrV is also provided (10). Translocators from the Inv-Mxi-Spa are not able to rescue translocation in *Yersinia*. The sequence identity between the translocators from the Ysc family and Inv-Mxi-Spa family is poor (less than 20%), and the *Shigella* and *Salmonella* translocators are considerably larger than the *Yersinia* or *P. aeruginosa* counterparts. These differences suggest that the proteins have evolved to adapt to a different mechanism of invasion and/or to interact with different host cell membranes. Therefore, one needs to be cautious when trying to extrapolate the properties observed for translocators from one family to the other.

Current models for the T3S translocon complex of the Ysc family are quite rudimentary, and they are mostly based on the following observations: (i) the translocators are found associated with cell membranes after incubating the pathogen in close contact with red blood cells (11); (ii) both translocators co-immunoprecipitate after Triton X-100 solubilization of membrane-associated proteins (11); and (iii) ring-like struc-

tures are observed using EM when the translocators are incubated with model membranes (12). The proteins are presumed to form a pore in which each PopB/YopB is speculated to have two transmembrane (TM) segments and each PopD/YopD only one TM segment based on sequence analysis (Fig. 1*A*). Both PopB and PopD can insert individually in model membranes and form discrete and stable pores, yet they interact with each other on the membrane when incubated together (13, 14). Other elements like coiled-coil segments and amphipathic α-helices can be predicted using bioinformatics analysis on PopB and PopD (Fig. 1*A*), however, how these proteins interact with other proteins or with the membrane is still uncertain.

We have established the experimental conditions necessary to maximize association and insertion of the *P. aeruginosa* translocators PopB and PopD into model membranes (14). Both proteins form pores in model membranes and allow the passage of small proteins and other molecules (13, 14). We sought here to provide specific insights about the stoichiometric arrangement and mechanism of assembly of the PopB and PopD translocators. Steady-state fluorescence spectroscopy of membrane-bound complexes indicated that when added together, PopB and PopD assemble hetero-complexes. Using single-molecule fluorescence photobleaching, we quantified the stoichiometry of membrane-assembled complexes. In the absence of PopD, PopB oligomers presented a bi-modal size distribution with peaks at 6 and 12 subunits. In the absence of PopB, PopD assembled mostly hexameric structures. Strikingly, when PopB and PopD were both present, they assembled into complexes containing 8 PopB and 8 PopD molecules. These findings provide the basis to explain the requirement of both translocators to assemble a functional TM hetero-complex with unique architecture.

Experimental Procedures

Protein Expression, Purification, and Characterization—The purification, structural characterization, and pore forming properties of isolated PopB and PopD were described before in detail (14). The expression and purification of hisPcrH-PopD, hisPcrH-PopB, their derivatives, and the isolation of the translocators from hisPcrH chaperone were done as previously described (14). The protein concentration was estimated using molar absorptivity of 18,910 M^{-1} cm^{-1} for hisPcrH, 13,980 M^{-1} cm^{-1} for PopD, 6,990 M^{-1} cm^{-1} and for PopB as described (14). Single Cys protein derivatives were obtained by site-directed mutagenesis. The functionality of the protein derivatives employed in these studies was evaluated by their ability to form pores in model membranes (14) and their ability to rescue translocation of *P. aeruginosa* PAK strain effectors into HeLa cells (15). PopB^{S164C} or PopD^{F223C} derivatives were able to rescue effector translocation in *P. aeruginosa* PAK strains with deletions for PopB (PAKΔ*popB*) or PopD (PAKΔ*popD*), respectively (Fig. 1). PAKΔ*popB* and PAKΔ*popD* deletion strains were generously provided by Dr. Stephen Lory. A synthetic 1494-bp DNA fragment (named GHD) encoding the *P. aeruginosa* PAK (Gene Bank AY232997.1) *pcrG* promoter (400–475), *pcrH* (1663–2179), and *popD* (3331–4231) was acquired from Biomatik. The construct was provided in the pUC57-Amp vector with an EcoRI site and a HindIII site at its

TABLE 1
PCR primers used to generate the pUCPHD and pUCPHB vectors

The pUCPHB vector was generated using Gibson assembly combining the Cys-less *P. aeruginosa* PA01 *popB* gene amplified from plasmid pETDuet1-hispcrHpopB (14) using primers 1 and 2; a fragment from GHD containing the *pcrG* promoter and *pcrH* gene amplified using primers 3 and 4; and the pUCP18 vector linearized by double digestion with EcoRI and HindIII. Vectors containing the genes codifying for PopD^{F223C} or PopB^{S164C} were generated similarly using Gibson assembly with the linearized pUCP18 vector and fragments obtained from pUCPHD or pUCPHB with primers 3 and 7, 6 and 5, or 3 and 9, 8 and 2, respectively.

	Primer sequences
1	5'–TCCGATAACGCTTGAACGCGCCGGACTGCCCTA
2	5'–GCCAGTGCCAAGCTTTCAGATCGCTGCCGGTCGG
3	5'–CTATGACCATGATTACGAATTCTGACGCAGCGAAGCCTGC
4	5'–TCAAGCGTTATCGGATTCATATGTTCG
5	5'–CGACGGCCAGTGCCAAGCTTCAGACCACTCCGGCCGC
6	5'–CAGTCCTGCGTCCAGATGGCCAACGC
7	5'–CTGGACGCAGGACTGGATCACCGTGTTG
8	5'–CCAGAAGTGCGGTCTGGCAGCCAAAATC
9	5'–CAGACCGCACTTCTGGGATTCTTTCGC

5' and 3', respectively. The GHD fragment was cut by double digestion with EcoRI and HindIII and cloned into the pUCP18 vector (generously provided by Dr. Dara Frank 16, 17) to generate the pUCPHD vector. The pUCPHB vector was generated by the Gibson assembly method (18) as instructed by the manufacturer (New England Biolabs) (Table 1). The infection assay was adapted from Kaufman *et al.* (15). Briefly, HeLa cells cultured in DMEM (Caisson) containing 10% FBS were maintained in a 37 °C incubator supplemented with 5% CO_2. Before infection, cells were washed once with pre-warmed PBS and incubated in fresh DMEM. Bacteria were grown overnight at 37 °C in Miller lysogeny broth, the next day the cells were diluted to an absorbance at 600 nm of 0.1 in fresh broth and grown until the absorbance reached a value of 1. To establish infection a bacterium/HeLa cell ratio of 30 was used. Bacteria were spun down at 16,000 × *g* for 2 min and suspended in 100 μl of DMEM, then incubated with HeLa cells grown to confluence in 6-well plates for 4 h at 37 °C (1.2 × 10^6 cells/well). The pore-forming activity of labeled derivatives was indistinguishable from the one observed for WT translocators (14).

Fluorescent Protein Labeling—PopB^{S164C} and PopD^{F223C} were labeled using the iodoacetamide derivative of BodipyFL (BpyFL C_1-IA, Invitrogen) as previously described (14). PopD^{F223C} was labeled using Bodipy® TMR C_5-Maleimide (BpyTMR, Invitrogen) using the same described procedure (14). Labeling efficiencies were calculated using the molar absorptivities at 280 nm in urea 6 M for PopB and PopD (see above), at 502 nm for BpyFL (55,000 M^{-1} cm^{-1}), and at 540 nm for BpyTMR (51,120 M^{-1} cm^{-1}). Protein concentration was calculated after correcting the absorbance by the contribution of the fluorescent dyes at 280 nm. The absorbance of BpyFL at 280 nm was 4% of its absorbance at 502 nm. The absorbance of BpyTMR at 280 nm was 20% of its absorbance at 540 nm. The percentage of labeling of selected preparations used for single molecule experiments were 96% for PopD$^{F223C-BpyFL}$, 100% for PopB$^{S164C-BpyFL}$, and 95% for PopD$^{F223C-BpyTMR}$ (hereafter PopD^{BpyFL}, PopB^{BpyFL}, and PopD^{BpyTMR}, respectively). For single-molecule experiments the labeled proteins were kept in the dark and all incubations were done in the absence of light to avoid photobleaching. To avoid bleaching of protein complexes during focusing of the sample prior to a photobleaching experiment, the focal plane containing single TM complexes was

found manually and a Perfect Focus System (PFS®, Nikon) was activated. This system monitors the position of the focal plane using a dedicated near infrared 870-nm light-emitting diode and line charge-coupled device sensor that adjusts focus automatically in milliseconds given a drift event in the *Z*-axis. After focusing and perfect focus system activation, laser excitation was turned off, the objective lens was moved to a new region never exposed to light, and the single-molecule photobleaching experiment was initiated acquiring the fluorescence emission from time 0 without requiring pre-focusing of the sample.

Liposome Preparation—Liposomes were prepared using identical composition and procedures previously described (14). NBD-PE (*N*-(7-nitrobenz-2-oxa-1,3-diazol-4-yl)-1,2-di-hexadecanoyl-*sn*-glycero-3-phosphoethanolamine) was purchased from Life Technologies.

Liposome Flotation-Membrane Binding Assay—Association of PopB and PopD to liposomes at the indicated pH was assessed by flotation of proteoliposomes through a sucrose gradient, SDS-PAGE, and quantification of the bound proteins by gel densitometry as described previously (14). When added together, PopB and PopD were pre-mixed in 6 M urea at the indicated ratio.

Supported Lipid Bilayers (SLB)—Clean glass coverslips were prepared by boiling coverslips in a 10% (v/v) solution of 7X® detergent (MP Biomedicals) for 20 min. Coverslips were then extensively washed with tap water, followed by extensive wash with pure water, followed by 10 min boiling in pure water. Dried coverslips were heated for 4 h at 400 °C in a kiln oven and stored until use. SLB were formed as follows: a sample containing 400 μl of liposome or proteoliposome (50 mM sodium acetate buffer, pH 4.0, 0.22 mM final lipid concentration, and 5 mM $CaCl_2$) was placed on a Petri dish between two 1-mm thick aluminum spacers. A clean glass coverslip was placed on top of the sample and incubated for 30 min to allow SLB formation. After this, a glass slide was placed next to the coverslip and the Petri dish was filled with buffer. While submerged in buffer, the coverslip was mounted on the glass slide spaced by two strips of double-sided adhesive tape to form a chamber.

Assembly of Protein Complexes for Imaging—For homo-oligomer reaction mixtures (100 μl) containing liposomes (0.1 mM total lipids) and BpyFL-labeled PopB or PopD (30 nM total protein) were incubated in buffer, 50 mM sodium acetate, pH 4.0, at 20–23 °C for 15 min (protein to lipid ratio 1/3,333). For dual labeled hetero-oligomers reaction mixtures were done similarly but total lipid concentrations were 0.3 or 0.6 mM and labeled proteins were 30 nM each (total protein to lipid ratio 1/5,000 or 1/10,000). Before assembly into SLB, proteoliposomes were diluted by addition of 1390 μl of buffer, 50 mM sodium acetate, pH 4.0, plus 10 μl of a solution of liposomes (30 mM total lipids stock concentration). For single-color labeled hetero-oligomers reaction were done similarly as for dual-color labeled ones, maintaining a total protein to lipid ratio of 1/4,550.

Imaging—Single molecule images were acquired using an electron multiplier charge-coupled device Cascade II camera (Photometrics, Tucson, AZ). Total internal reflection fluores-

cence (TIRF) microscopy used a home-built laser system around a Nikon Eclipse Ti microscope and a high numerical aperture objective ($\times$60, NA 1.49) (Nikon, Melville, NY). TIRF excitation was achieved using a 488-nm argon-ion air laser (Melles-Griot) for PopD^{BpyFL} and PopB^{BpyFL}, and a 532-nm solid state (Crystalaser) laser for PopD^{BpyTMR}. Neutral density filters were employed to attenuate laser light to the desired level and increase the average photobleaching time. The standard exposure and acquisition interval time was 70 ms for BpyFL and 100 ms for BpyTMR probes. Dual-color photobleaching was performed first by constant illumination from a 532-nm laser line to photobleach the red emitting dye BpyTMR, followed by constant illumination with a 488-nm laser line to photobleach the green emitting BpyFL. The consecutive photobleaching of BpyTMR followed by BpyFL was done to minimize any problems associated with potential FRET between the dyes and any direct excitation or photobleaching of BpyTMR when using the 488-nm wavelength. Time point image stacks were independently acquired for PopD^{BpyTMR} and PopB^{BpyFL}, and emission intensity as a function of the illumination time was analyzed for individual protein complexes.

Single-molecule Photobleaching—Photobleaching of labeled translocators was performed on SLB assembled using liposomes with membrane-inserted proteins. Photobleaching data were inspected and analyzed manually. Diffraction-limited spots in image stacks were identified and quantified over time using ImageJ. Time-resolved fluorescence intensity plots of single protein complexes were generated importing the measured intensities into Origin software. The number of fluorescent molecules in each complex was obtained by dividing the background-subtracted initial fluorescence intensity by the intensity contribution of a single dye revealed by single stepwise photobleaching events, most frequently discernible within the last few photobleaching events within each trace (19, 20). Single monomers were not considered in our analysis given the difficulty of distinguish them from background noise. Because $\sim$100% of the proteins were labeled, and we were able to temporally separate the bleaching of a single fluorophore, the overall photobleaching corresponded to the presence of all the subunits of the complex. This is the ideal situation for photobleaching enabling each subunit to be directly counted without the need to implement discrete statistical distributions to deduce the number of molecules in the complex.

Steady-state Fluorescence Spectroscopy—Steady-state fluorescence measurements and spectra for fluorophore characterization and quantification were collected using a Fluorolog 3–21 spectrofluorometer as described earlier (14). Anisotropy and emission intensity measurements were taken using a Chronos fluorescence lifetime spectrometer (ISS, Champaign, IL) equipped with a 470-nm laser diode and Glan-Thompson prism polarizers (10 $\times$ 10 mm aperture for excitation and 14 $\times$ 14 mm aperture for emission) (14). Emitted light was collected through a Melles Griot cutoff glass filter GG495 to eliminate scattered light. All measurements were blank subtracted with an equivalent sample lacking the fluorophore. For emission intensity measurements the amount of PopD^{BpyFL} was kept constant (final concentration 10 nM) and the amount of WT PopD (PopD^{WT}) or PopB^{WT} adjusted to render the indicated
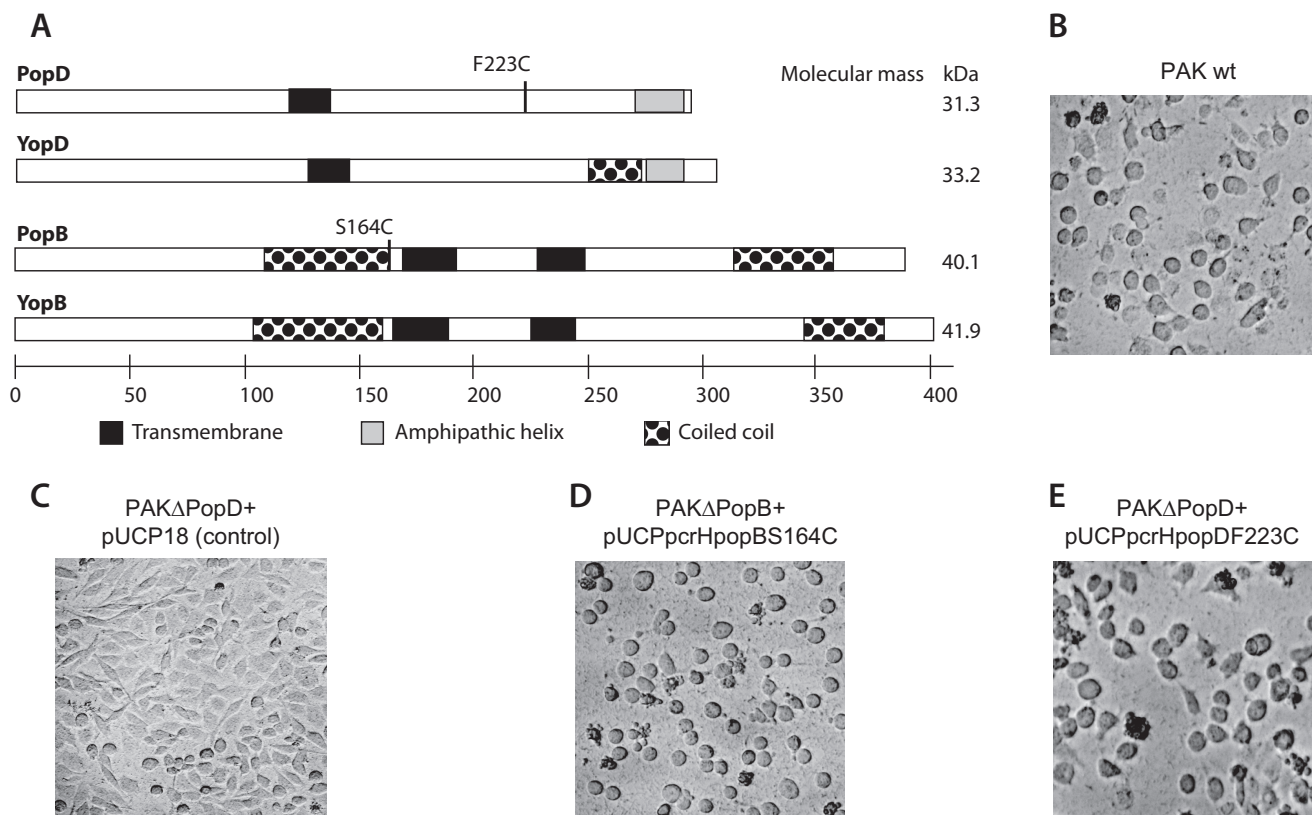
FIGURE 1. **PopB^{S164C} and PopD^{F223C} derivatives were active for effector translocation.** *A,* scheme of the primary structure of *P. aeruoginosa* PAO1 translocators PopD (gi 9947683) and PopB (gi 9947682) compared with the homologue *Y. enterolcolitica* translocators YopD (gi 586795) and YopB (gi 122815801). Location of the single Cys modifications introduced for probe labeling is indicated on PopD and PopB. Predicted hydrophobic segments, amphipathic helices, and coiled coils are shown. The molecular mass for each translocator is shown on the *right*. The scale at the *bottom* indicates amino acid number. The activity of the PopB (or PopD) derivative was indistinguishable from the wild-type protein when evaluated for their ability to complement a popB deletion strain (or a popD deletion strain). The activity of the translocators was assessed by the characteristic rounding up of the infected target cells due to actin cytoskeleton disruption caused by effector translocation (15). Strains used in this assay were *P. aeruginosa* PAK WT (*B*), PAKΔpopD complemented with pUCP18 (*C*), PAKΔpopB complemented with pUCPHB^{S164C} (*D*), and PAKΔpopD complemented with pUCPHD^{F223C} (*E*). The PAKΔpopB control showed no effect on cell morphology as shown for the PAKΔpopD control in *panel C* (not shown).

percentage of labeled protein. The protein:lipid ratio was kept constant at 1/3,000 or 1/10,000 by adjusting the amount of lipids added. For anisotropy measurements total protein concentration was kept constant at 100 nM and total lipid concentration at 1 mM. The percentage of labeling was adjusted by premixing PopD^{BpyFL} with PopD^{WT} (or PopB^{WT}) in 6 M urea. BpyFL was excited with polarized light, and both vertically polarized (∥) and horizontally polarized (⊥) emission intensities were recorded. Anisotropy was calculated using $r = (I∥ - I⊥)/(I∥ + 2I⊥)$, where I is the background-subtracted emission intensity of vertically (or horizontally) polarized light. While working with membrane bilayers it is important to select experimental conditions where the anisotropy (homoFRET) signal originates from the association of proteins, and not as a result of the proximity of randomly distributed proteins. Based on determinations of liposome size by electron microscopy (14), and the protein:lipid ratio used in these studies, we estimated that randomly distributed proteins will be on average more than 200 Å apart in our system.

Time-resolved Fluorescence Spectroscopy—Lifetime measurements were done using a Chronos fluorescence lifetime spectrometer (ISS, Champaign, IL) as described previously (14).

Results

PopB Assists the Association of PopD with Membranes—Both PopB and PopD can efficiently form stable pores at acidic pH on liposomes containing negatively charge phospholipids (12). In addition to their individual ability to insert into membranes, we have shown that the translocators can also interact with each other and form hetero-oligomers that span the bilayer (14). To examine the molecular mechanism of PopB-PopD interactions, we investigated the association of the translocators when simultaneously binding to membranes over a broad pH range, expanding from the optimal acidic pH to neutral conditions.

A single Cys residue was introduced into each translocator at a location predicted to be solvent-exposed (Fig. 1A), and specifically labeled with the fluorescent probe BpyFL. Labeled PopB and PopD were incubated with membranes at the indicated pH, and the association of proteins with lipid bilayers was determined using a liposome flotation assay. The membrane-containing fraction was analyzed by SDS-PAGE and membrane-bound proteins were quantified using gel densitometry (Fig. 2A). In this assay only liposomes and proteoliposomes float to the top of the gradient, whereas free proteins or protein aggregates remain in the bottom fraction. To detect any coop-

A

	Total					pH				
	protein	4.0	4.5	5.0	5.25	5.5	5.75	6.0	7.0

PopB

PopD

PopB plus PopD

B

C
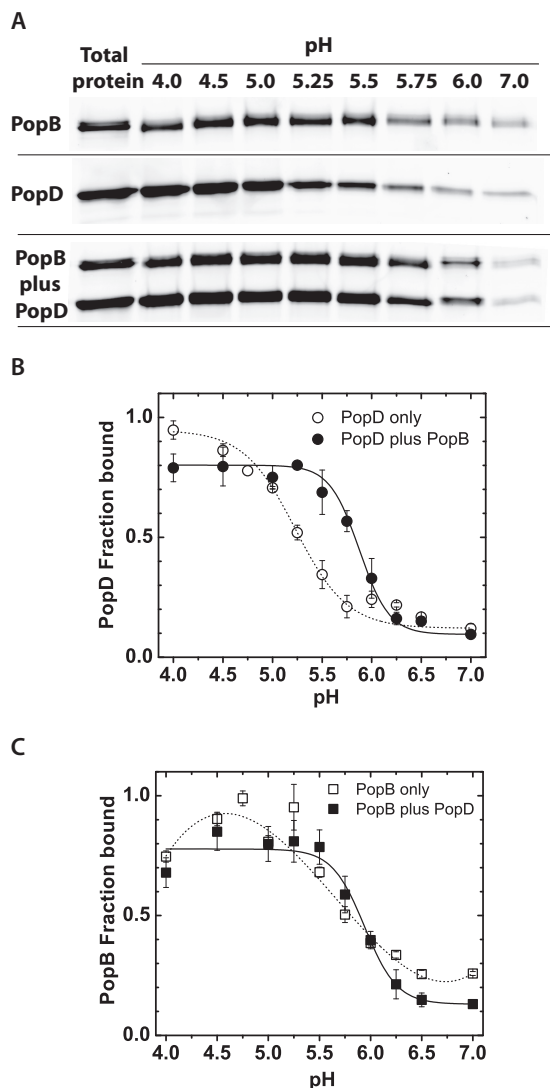
FIGURE 2. **PopB enhanced PopD membrane binding.** *A,* SDS-PAGE gel showing the amount of purified PopD^{BpyFL} and/or PopB^{BpyFL} isolated in the membrane containing fraction after bound and unbound proteins were separated using a liposome flotation membrane-binding assay as described in the text. Total lipids were 2 mm and total protein was 400 nm. Individual proteins or pre-mixed proteins were incubated with membranes at 20–23 °C for 1 h before ultracentrifugation using a sucrose gradient. Proteins were visualized using BpyFL fluorescence. *B,* PopD^{BpyFL} binding at the indicated pH when the translocator was incubated with membranes alone or when premixed and incubated with an equimolar amount of PopB^{WT}. *C,* PopB^{BpyFL} binding at the indicated pH when the translocator was incubated with membranes alone or when premixed and incubated with an equimolar amount of Pop-D^{WT}. BpyFL fluorescence was quantified by gel densitometry and each data point represents the average of at least two independent assays and *error bars* indicate the data range. Average lines to individual translocators (*dashed*) and both translocators (*solid*) are shown only as a guide for the reader.

erative interaction between PopB and PopD, their membrane association was first quantified for individual translocators and then when the two translocators were added together. Any difference in the binding properties of PopB or PopD when incubated alone or in combination suggest a potential interaction between the translocators.

Membrane association for PopD was higher than 90% at pH 4.0, 50% around pH 5.3, and minimal at neutral pH (Fig. 2*B*). Interestingly, when PopD and PopB were mixed in equimolar

amounts prior to incubation with membranes, the binding of PopD was significantly enhanced in the 5.2–5.8 pH range. PopB membrane association was higher than 90% at pH 4.8, 50% around pH 5.8, and less than 30% at neutral pH. PopB membrane binding was not significantly affected by the presence of PopD (Fig. 2*C*).

These results suggested that the simultaneous addition of PopB and PopD influences how the proteins interact with membranes, and we hypothesized that this affects their final membrane-inserted arrangement. We therefore focused our analysis on the ability of each translocator to form oligomers on membranes when added individually or combined. We characterize the assembly of membrane complexes at pH 4.5, where binding to membranes reached saturation.

PopD and PopB Form Multimers on Lipid Membranes— FRET or homoFRET (FRET between like molecules), as a function of fractional fluorescent labeling, has been used to determine the oligomerization state of small protein complexes (21). When homoFRET occurs, energy can migrate from dye to dye before a photon is emitted, thereby depolarizing the light and reducing the anisotropy of the sample. How much depolarization occurs depend, among other parameters, on the distance among dyes. Therefore, the steady-state fluorescence anisotropy signal reports on the efficiency of homoFRET (*i.e.* the distance) between protein molecules labeled with the same fluorophore. In addition to homoFRET, the fluorescence anisotropy can also be influenced by changes in the rotational diffusion of the labeled protein. However, this source of ambiguity is overcome by analyzing anisotropy as a function of the molar fraction for the labeled protein when diluted with unlabeled protein. Under these conditions, changes in fluorescence anisotropy are due to differential separation between the fluorescent probes and reflect on the size of the protein oligomer (21). Both homo- and hetero-oligomerization can be assessed using this approach (22).

In addition to the relatively long range distance information provided by homoFRET measurements ($R_0 \sim 50$ Å), BpyFL dyes can form non-fluorescent dimers when positioned a few angstroms apart, which is easily detected by a decrease in the fluorescence intensity, and reports on molecular interactions within a shorter distance range compared with homoFRET (23). BpyFL self-quenching is indicative of adjacent subunits because orbital contact between fluorophores is required (24), and this effect has been exploited in various analytical methods, like biotin-avidin binding detection (25) and single molecule folding studies (26). Moreover, BpyFL is especially useful to study protein-membrane interactions because its fluorescence properties are not sensitive to the pH or polarity of the environment (27, 28).

The ability of PopD to interact with other PopD molecules or with PopB prompted us to investigate the nature of the oligomers formed by these proteins. For PopD-PopD interactions, both the anisotropy (homoFRET) and fluorescence intensity (self-quenching) were measured as a function of the fraction of labeled PopD^{BpyFL} present, which was controlled by addition of PopD^{WT}. Although keeping the total amount of fluorophore constant, an increase in the emission (de-quenching) was observed as the fractional amount of PopD^{BpyFL} was reduced,
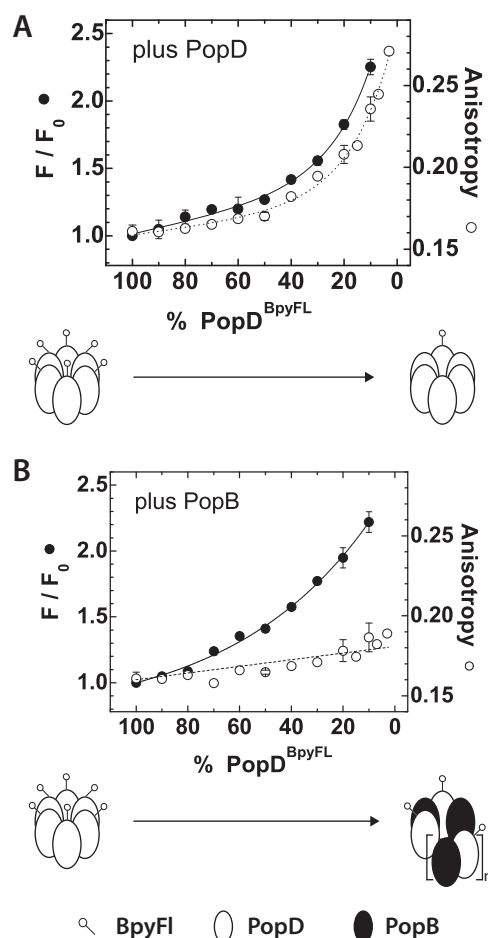
FIGURE 3. **PopD assembled homo- or hetero-oligomeric structures in membranes.** Fluorescence intensity and anisotropy changes observed upon the dilution of PopD^{BpyFL} with increasing amounts of PopD^{WT} or PopB^{WT}. *A*, steady-state fluorescence intensity and anisotropy of PopD^{BpyFL} measured at the indicated percent of labeled protein when diluted with PopD^{WT}. *B*, steady-state fluorescence intensity and anisotropy of PopD^{BpyFL} when diluted with PopB^{WT}. Scheme indicating the labeled PopD^{BpyFL} distribution expected for complexes containing 100% labeled PopD or a mixture of proteins containing 3% labeled PopD^{BpyFL}, are shown at the *bottom* of each figure. PopD complexes were drawn as hexamers and hetero-complexes as (PopD-PopB) *n*-mers for simplicity. *Error bars* represent the data range of at least two independent assays. Average lines are shown as a guide for the reader.

clearly indicating that PopD formed oligomers on membranes (Fig. 3*A* and Table 2). At the same time, the homoFRET between subunits decreased (*i.e.* increase in fluorescence anisotropy) when the fractional amount of PopD^{BpyFL} was reduced.

The interaction of PopD with PopB was explored using a similar approach. While keeping a constant amount of PopD^{BpyFL}, PopB^{WT} was added in increasing amounts. Emission measurements revealed that PopD^{BpyFL} associated with PopB as efficiently as with PopD, because the same final recovery of the fluorescent intensity was observed when the molar fraction of PopD^{BpyFL} was decreased (Fig. 3*B* and Table 2). In contrast, very little decrease in homo-FRET (*i.e.* increase in fluorescence anisotropy) took place when the molar fraction of PopD^{BpyFL} was reduced using PopB^{WT}. These results suggested that PopB was able to intercalate between PopD subunits (as shown by the decrease in the BpyFL self-quenching), but the

longer range homoFRET still occurred among subunits in a complex. Given that PopD^{BpyFL} efficiently interacts with PopB, the lack of increase in anisotropy was indicative of the presence of at least two or more PopD^{BpyFL} subunits per PopB/PopD hetero-complex. Taken together, these results showed that PopD assembles homo-oligomeric structures in membranes, but when added together with PopB it forms hetero-oligomeric structures of yet undetermined size and stoichiometry.

Individual Translocators Adopt Mostly Hexameric Arrangements When Assembled into Lipid Bilayers—To effectively determine the stoichiometry of membrane-inserted oligomers and the heterogeneity of the samples, we applied single-molecule fluorescence photobleaching. This technique allows for quantification of the number of protein molecules within a protein complex (19, 29). In practice, fluorescence detection with single-molecule efficiency allows visualization of single photobleaching events as a stepwise decrease in the fluorescence signal. The high sensitivity of this technique combined with the spatial resolution of optical microscopy imaging of single protein complexes, allowed us to quantify the number of photobleaching events occurring in a single membrane inserted oligomer (Fig. 4). The number of photobleaching events is equivalent to the number of fluorophores attached to a protein complex, or in the case of single-labeled polypeptides, to the number of proteins forming part of the complex. We adapted the technique to quantify proteins in their native lipid bilayer environment (*i.e.* in the absence of detergents) by using SLB (30).

PopB^{BpyFL} or PopD^{BpyFL} were reconstituted into liposomes using previously optimized conditions for membrane association and pore formation (14). The resulting proteoliposomes were diluted with excess liposomes to achieve the optimal low protein density required for single-particle imaging. Diluted samples were used to assemble SLB on glass coverslips by the vesicle fusion method (31). Bilayers were imaged using single-molecule TIRF microscopy as detailed under "Experimental Procedures."

Assembly of a continuous and fluid lipid bilayer was confirmed in a parallel experiment by including a fluorescently labeled phospholipid in the membranes, NBD-PE, and observing fluorescence recovery after photobleaching of a membrane patch. Fluorescence recovery after photobleaching under our experimental conditions occurred in a time scale consistent with phospholipid diffusion in a fluid lipid bilayer (calculated 10^{-12}-10^{-11} m^2/s lateral diffusion coefficient for NBD-PE, data not shown) (32). In contrast to the freely diffusing lipid molecules, protein complexes remained immobile during the time scale of visualization before complete photobleaching of the attached probes (no significant drifting of the fluorescence complex was observed on membranes). This behavior has been observed for integral membrane proteins inserted into SLB, presumably due to interaction or absorption of the protein to the glass surface caused by protein segments facing the glass side of the membrane (33).

A quantitative analysis of photobleaching steps from 100 individual PopD oligomers and more than 150 individual PopB oligomers was employed to determine the stoichiometry of complexes formed by PopD (or PopB) when assembled into

TABLE 2
Average fluorescence lifetimes of BpyFL in homo- and hetero-oligomers at varying percent of the fluorescent label

Proteoliposome preparations containing the same protein and lipid concentration, while varying the molar fraction of PopD[BpyFL] and either PopD or PopB (see Fig. 3), were analyzed using frequency-domain fluorescence spectroscopy as described previously (14). Phase-Delay and Modulation-Ratio data points for each individual sample were fit to a double-exponential decay model. Addition of a third exponential decay component did not significantly improved the fit. The table summarizes the Intensity weighted ($\langle \tau \rangle^I$) and Amplitude weighted ($\langle \tau \rangle^A$) average fluorescence lifetimes derived from each individual best fit (in nanosecond time units), as well as the reduced chi-squared (χ^2) goodness of fit test parameter.

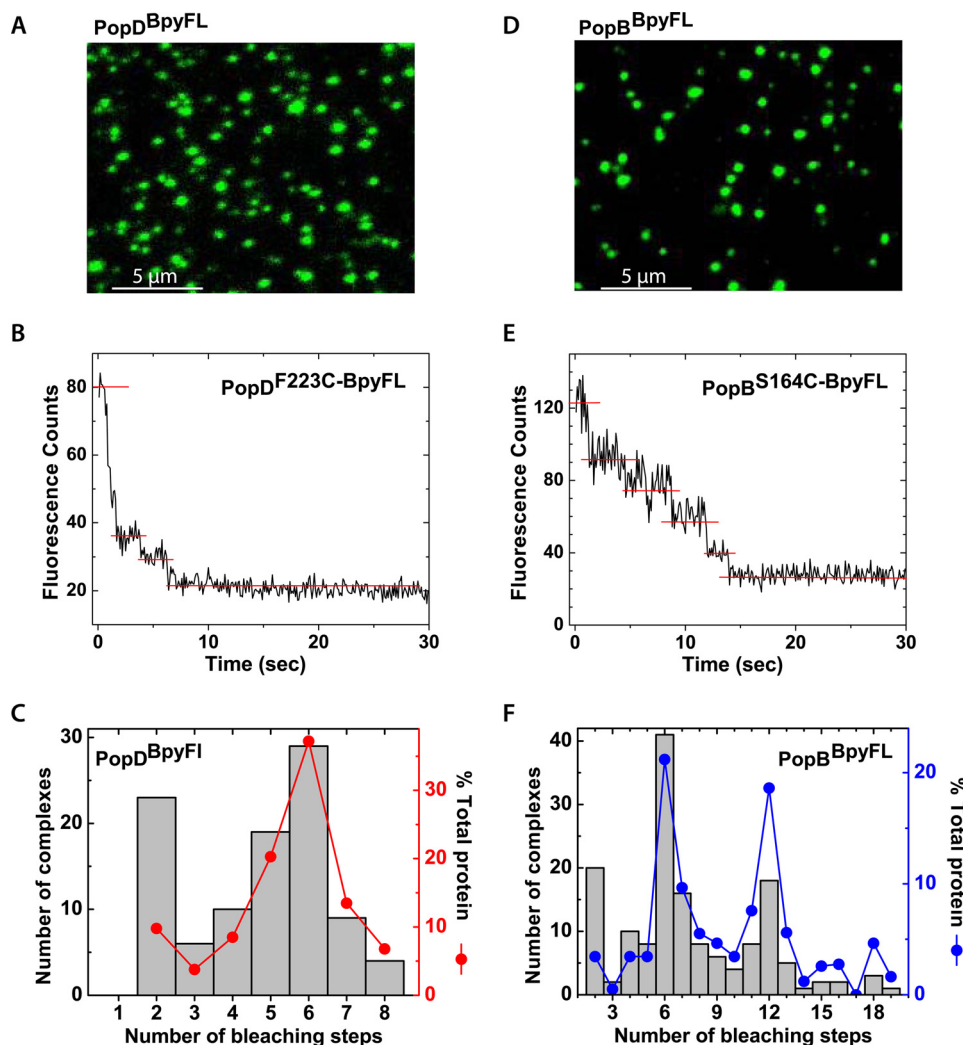| % PopD[BpyFL] in sample		100	90	80	70	60	50	40	30	20	10
Plus PopB	$\langle \tau \rangle^I$	4.8	4.9	5.1	4.7	5.2	5.2	5.4	5.3	5.5	5.6
	$\langle \tau \rangle^A$	3.2	3.2	3.6	3.2	3.9	4.0	4.5	4.7	5.1	5.3
	χ^2	5	5	5	5	3	3	2	1	1	1
Plus PopD	$\langle \tau \rangle^I$	4.8	4.7	5.1	4.8	4.6	4.7	4.6	4.7	4.9	5.2
	$\langle \tau \rangle^A$	3.3	3.2	3.6	3.3	3.2	3.4	3.4	3.7	4.3	4.9
	χ^2	3	3	5	3	2	2	2	1	1	1

FIGURE 4. **PopD and PopB adopt mostly hexameric arrangements when assembled individually in membranes.** *A*, TIRF microscopy image of PopD[BpyFL] complexes in SLB. *B*, example of an intensity time trace obtained from a single membrane-assembled PopD[BpyFL] complex. Single-molecule photobleaching events were evidenced by the stepwise decrease in the fluorescence intensity. *C*, quantification of photobleaching counts obtained from 100 time traces of single PopD[BpyFL] complexes. *D*, TIRF microscopy image of PopB[BpyFL] complexes in SLB. *E*, example of an intensity time trace obtained from a single membrane-assembled PopB[BpyFL] complex. *F*, quantification of photobleaching counts obtained from 155 time traces of single PopB[BpyFL] complexes. *Filled dots* in *C* and *F* represent how much of the total protein represented in the figure was present in each of the bleaching steps groups.

membranes. More than 70% of the total PopD translocators were found in complexes formed by 6 ± 1 subunits, indicating that PopD[BpyFL] assembled mostly hexameric structures when incubated alone with membranes (Fig. 4*C*). For PopB, a broader size distribution was observed dominated by hexameric and dodecameric oligomers (Fig. 4*F*).

PopB and PopD Assemble Hexadecameric Hetero-complexes in Membranes—To effectively determine the stoichiometry of hetero-oligomers we applied a technique that allows for quantification of the number of different protein molecules within a single protein complex (19). Dual-color fluorescence photobleaching was used to simultaneously determine the number of
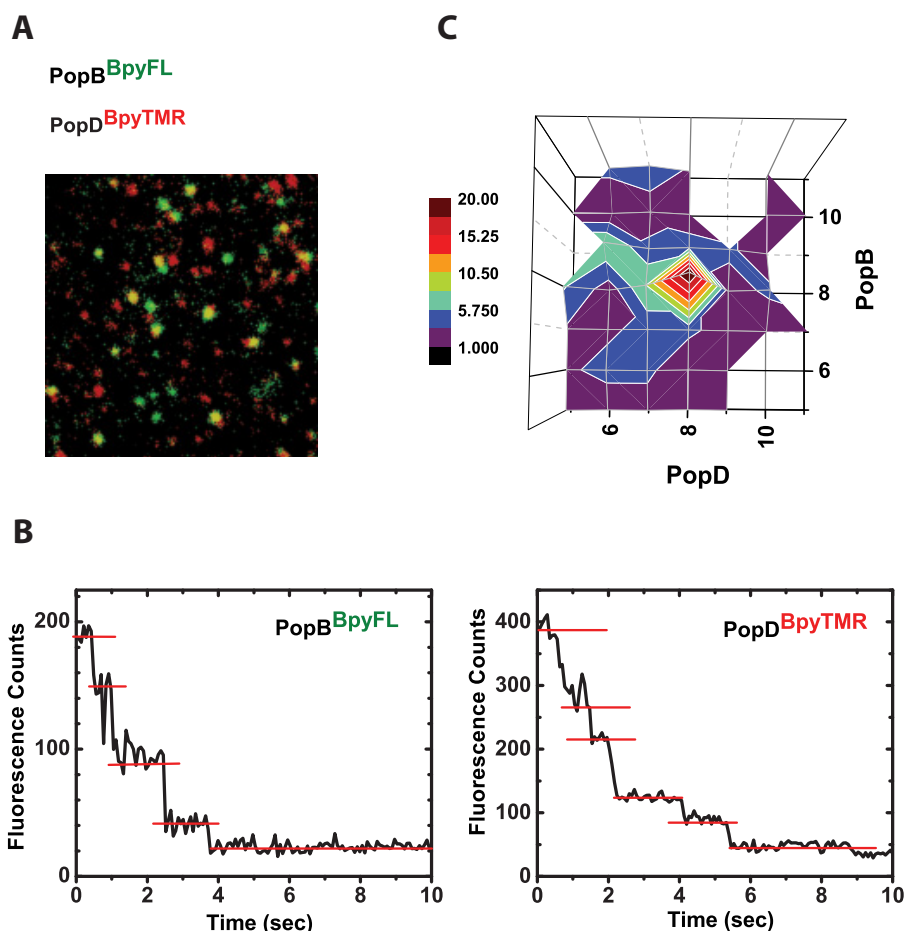
FIGURE 5. **PopB and PopD assemble hexadecameric hetero-complexes in membranes.** Protein complexes resulting from the equimolar addition of PopD^{BpyTMR} (*red* emitting) and PopB^{BpyFL} (*green* emitting) were imaged using dual color single-molecule TIRF microscopy on SLB. *A,* merge image of single particles containing PopD^{BpyTMR} (*red*) and PopB^{BpyFL} (*green*). *Yellow spots* indicate co-localization of PopD^{BpyTMR} and PopB^{BpyFL} in individual complexes. *B,* typical fluorescence intensity time traces for single protein complexes. Photobleaching events appear as stepwise decrease in the intensity. *C,* quantification of dual-color photobleaching counts obtained from 226 time traces of particles containing both PopD^{BpyTMR} and PopB^{BpyFL}. The heat map for observed PopD:PopB distributions is centered at 8 photobleaching counts for PopD and 8 photobleaching counts for PopB.

PopB and PopD molecules present in membrane-assembled oligomers. Each translocator was quantified based on the unique properties of the different fluorescence dyes covalently attached to them. PopD^{F223C} was labeled at ~100% efficiency with the red-emitting fluorescent probe BpyTMR, whereas PopB^{S164C} was labeled with same efficiency using the green emitting fluorescent probe BpyFL. Control experiments showed that no labeling occurred on WT translocators (which lack Cys residues) when they were incubated with labeling reagents (14).

PopB^{BpyFl} and PopD^{BpyTMR} were mixed and reconstituted into liposomes, and SLB were prepared as described above. This technique permitted the analysis of hetero-complexes regardless of the presence of co-existing homo-oligomers of PopB and PopD, as only hetero-complexes display co-localization of green (PopB) and red (PopD) fluorescence (Fig. 5*A, yellow spots*).

A quantitative analysis of the time-dependent photobleaching for more than 220 individual protein complexes showing yellow spots was used to determine the stoichiometry of oligomers formed by both PopD and PopB (Fig. 5*B*). Remarkably, we found that the distribution of PopB·PopD complexes centered at 8 photobleaching counts for PopD^{BpyTMR}, as well as 8 photobleaching counts for PopB^{BpyFL} (Fig. 5*C*), constituting an hexadecameric complex. This stoichiometry was independent of the total amount of protein distributed on the vesicles because identical results were obtained when the experiment was done using a 2-fold higher protein:lipid ratio (1/10,000, data not shown).

Individual PopD and PopB homo-oligomers were still observed under these experimental conditions (when the PopB: PopD ratio was 1/1), but it was clear that the proteins arranged into a different oligomeric structure when interacting with each other. The ability of the proteins to form both homo- and hetero-oligomers prompted us to analyze the reversibility of formed complexes. We therefore analyzed if the formation of PopD homo-oligomers was reversible after addition of PopB taking advantage of the PopD^{Bpy} self quenching properties. As showed in Fig. 3*B*, the emission of PopD^{Bpy} was low when forming homo-oligomers (Bpy self quenching), but increased when PopD^{Bpy} was pre-mixed with an excess of PopB before their addition to the membranes. However, if excess PopB was added after the PopD^{Bpy} homo-oligomers were formed, no change in the emission of Bpy was observed (Fig. 6*A*). This suggested that
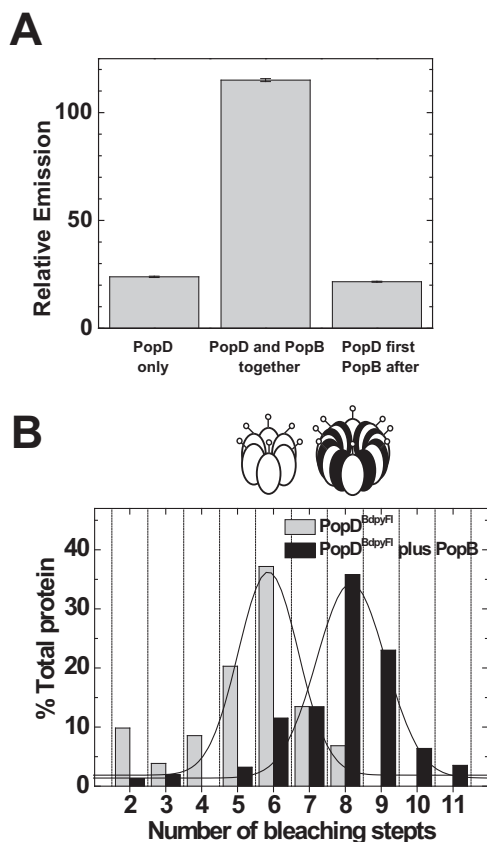
FIGURE 6. **Simultaneous membrane interaction favored hetero-oligomer- ization over formation of translocator homo-oligomers.** *A,* formation of the PopD homo-oligomer is not reversed by PopB addition to membranes. *Left bar,* PopD^{BpyFL} was incubated with membranes and the final self- quenched emission determined (PopD only). *Center bar,* PopD^{BpyFL} was mixed in 6 M urea buffer with a 10-fold excess of PopB^{WT} and the mixture was added to membranes. Excess PopB favored the incorporation of PopD into hetero-oligomers, therefore it de-quenches the emission of the BpyFl probe (see also Fig. 3*B*). *Right bar,* PopD^{BpyFL} was incubated with membranes to allow homo-oligomer formation and a 10-fold excess of PopB was subse- quently added. No emission de-quenching was observed in this case, indicat- ing that the simultaneous interaction with membranes of both translocators is necessary to form hetero-oligomers. A constant amount of PopD^{BpyFL} (83% labeled with BpyFL) was present in every sample at a final concentration of 10 nM. The protein to lipid ratio was 1/6000 in all samples. *Error bars* indicate the range between two measurements. *B,* PopD size distribution shifts from 6 to 8 subunits per complex when membrane incubation is done in the presence of PopB. PopD^{BpyFL} was incubated with membranes in the presence of 10-fold excess PopB whereas maintaining a constant protein:lipid ratio (*black bars*). Size distributions were obtained using single-molecule photobleaching and compared with the distribution obtained when PopD^{BpyFL} was incubated alone with membranes (Fig. 4*C*, reproduced in *gray bars*). *Lines* indicate Gaussian fits to the histogram data. Oligomers are represented as coded in Fig. 3.

after assembling a homo-oligomer, the PopD subunits cannot dissociate and form a hetero-oligomer.

Because the assembly of PopD homo-oligomers is not revers- ible, how much of each complex would be formed in this model system is dictated by the relative rates of homo- *versus* hetero- oligomerization. By increasing the PopB/PopD ratio from 1:1 to 10:1 in the reconstitution assay, we were able to optimize the incorporation of PopD into hetero-complexes (Figs. 3*B* and 6*B*). Taken together, these data showed that although PopD is able to assemble stable hexamers on membranes, an early inter- action event between PopB and PopD along the assembly path-

way is required to secure the formation of a hexadecameric hetero-complex.

Discussion

Our spectroscopic analysis of reconstituted membrane pro- tein complexes has provided important insights into the struc- tural organization and assembly of the complex formed by the T3S translocators PopB and PopD. First, PopB facilitated the association of PopD with membranes. Second, in the absence of PopB, PopD formed mostly hexameric membrane complexes. Third, the interaction of PopB with PopD drove the formation of membrane-bound hetero-oligomer with a stoichiometry that differed from the one adopted by isolated proteins in homo-oligomers. Fourth, single molecule dual color photo- bleaching determinations showed that hetero-oligomers contained 8 PopB and 8 PopD subunits. Therefore, the inter- action of PopB with PopD during translocon assembly was critical to chaperone the formation of membrane-inserted hetero-complexes.

Negatively charged lipids and acidic pH have been often used to optimize the interaction of pore-forming toxins and other proteins with membranes *in vitro* (34–37). In some cases, acidic pH can induce a molten globular state in proteins due to changes on charged amino acids. This relaxed form may facili- tate membrane insertion (38). The exposure of hydrophobic surfaces by molten globular states at neutral pH favor protein aggregation in solution (as in the case of PopB and PopD (12, 13, 39)). However, the increase of the net positive charge of the protein at low pH would increase the electrostatic repulsion between proteins monomers and favor the electrostatic inter- action with negatively charged membranes. It is therefore not surprising that the association of purified PopB and PopD (*i.e.* in the absence of the needle complex) to model membranes requires acidic pH and is facilitated by the presence of anionic lipids (13, 14).

The hydrophobic character of PopB and PopD and their pro- pensity to aggregate in aqueous solutions demand a robust, reproducible, and controllable experimental system to study the structural arrangement of the T3S translocon. Unfolding- dependent membrane insertion is a reasonable approach because PopB and PopD are expected to be secreted unfolded through the narrow conduit of the T3S needle.

We therefore optimized the reconstitution of PopB and PopD membrane complexes by spontaneous refolding of urea- solubilized proteins in the presence of membranes (14). This folding-based reconstitution system allowed the study of indi- vidual WT translocators and to detect any difference in their properties that may result from the interaction between them. As shown in Fig. 2, when individually incubated with mem- branes, optimal binding for both PopB and PopD required pH lower than 5, however, PopB assisted the binding of PopD in a narrow pH range (*i.e.* pH 5–6).

The mechanistic details that govern the interaction between PopD and PopB are far from being understood. Mostly because no high resolution information is available on these proteins. However, the interaction between PopB and PopD was inde- pendently confirmed in this work using two spectroscopic properties of the fluorescent dye BpyFL, emission self-quench-

ing, and energy migration. Using these complementary approaches, we found that PopB formed hetero-oligomers with PopD[BpyFL] (Fig. 3B), and these complexes contained several PopD[BpyFL] subunits even when a high PopB:PopD[BpyFL] ratio was used. These observations suggest that the formation of a hetero-dimer may re-direct the assembly and architecture of the TM complexes.

We therefore employed TIRF microscopy and single molecule photobleaching (30, 40, 41) to determine the stoichiometry of homo- and hetero-oligomers formed by PopB and PopD inserted in membranes. These experiments clearly showed that a unique hetero-oligomer is formed when PopB and PopD are added together. These data are in good agreement with results showing that both translocators are required for effector translocation, and that both translocators have to be secreted from the same bacterium for translocation to take place (11). When secreted separately, the encounter between PopB and PopD may take too long and homo-oligomerization dominates under these conditions.

Hetero-oligomers formed by PopB and PopD contained mostly 8 PopB and 8 PopD molecules (Fig. 5C), indicating that the presence of both translocators in a particle was not simply a random distribution of translocators or a co-localization of individual homo-oligomers (which are mostly hexameric, Fig. 4). It is worth noting that a translocon complex containing 8 PopD molecules and 8 PopB molecules will have a molecular mass of 570 kDa (or 601 kDa for a YopD$_8$YopB$_8$, see Fig. 1). Therefore, the molecular mass obtained using this model system is in good agreement with the molecular mass roughly estimated for *Yersinia* translocons isolated from erythrocyte membranes using blue native gel electrophoresis (600 ± 100 kDa) (42). Taken together, single molecule fluorescence and ensemble experiments suggest a model where the interaction of PopD with PopB, presumably a dimer formation, leads to the assembly of unique hetero-oligomeric structures with defined stoichiometry on lipid bilayers. We can speculate that the sequential secretion of PopB and PopD in the proximity of the target membrane would favor the formation of hetero-oligomers in the proximity of the needle tip. The tip may facilitate the PopB-PopD association and chaperone their insertion into the membrane (4, 43, 44). Unfortunately, the hierarchical mechanism of secretion for the translocators is far from being understood.

Some advances have been made on the assembly of the *Shigella* counterparts IpaD, IpaB, and IpaC (equivalents to PcrV, PopB, and PopD in *P. aeruginosa*, respectively (45–47)). However, as mentioned above given the poor sequence identity among the translocators from the Inv-Mxi-Spa and the Ysc families, it is risky to extrapolate results obtained from one family to the other (48). In particular, when these bacteria have evolved to invade different organs and to interact with different cell types. For example, in the *Shigella* system, binding of bile salts trigger IpaB association with the tip and secretion of IpaC. After secretion, the interaction of IpaC with membranes is required to complete the association of the membrane-associated translocator with IpaD/IpaB at the needle tip (49). In contrast, neither YopB nor PopB are found associated with the tip of the needle (50). Moreover, *P. aeruginosa* strains where PopD is absent cannot translocate effectors, but PopB is still found

associated with the target membrane (11). It is therefore clear that the translocators evolved to adapt to different cell targets, and their functions may differ among different families.

Although homogeneous hetero-complexes were observed on membranes when PopB and PopD are added in equimolar amounts, a great number of homo-complexes were also observed (Fig. 5A). Are there any physiological role(s) for homo-oligomers? It has been claimed that in addition to the essential role in effector translocation, homo-oligomerization of IpaC (or SipC in *Salmonella*) is essential for events that occurs inside the cytoplasm of the target cell. For example, SipC initiates actin nucleation (51) and IpaC has the ability to induce membrane extensions on macrophages (52, 53). Moreover, IpaB induces Golgi fragmentation and reorganization of the recycling compartment (54) and oligomerization of IpaB form channels that permit potassium influx within endosomal compartments (55). Thus, it is possible that homo-oligomerization of PopD and PopB play other roles in the cytosol of the infected cell, but such abilities remain to be identified for the Ysc family members.

Finally, we would like to emphasize the unique properties of the T3S translocators in the context of protein membrane insertion and folding. Proteins that insert into membranes can be broadly classified in two major groups: (i) those that insert as unfolded polypeptides and require a complex proteinaceous machinery to properly fold and assemble into the lipid bilayer (56, 57), and (ii) those that spontaneous insert but are secreted as well folded proteins, as best exemplified by bacterial pore-forming toxins and complement system proteins (58–60). The T3S translocators do not belong to any of these groups. They are secreted through the needle in an unfolded conformation (61), they do not adopt a well defined folded structure in aqueous solution (39, 62), and no proteinaceous machinery has been identified for insertion and assembly into the target membrane. Therefore, the spontaneous assembly of unfolded proteins into large hetero-complexes with a defined stoichiometry constitutes a novel paradigm among membrane inserted proteins. As shown here, early interactions between PopB and PopD that occur during refolding, membrane binding, and/or insertion direct the spontaneous assembly of a hetero-complex of defined stoichiometry in a membrane bilayer.

References

1. Cornelis, G. R. (2006) The type III secretion injectisome. *Nat. Rev. Microbiol.* **4,** 811–825

2. Galán, J. E., and Wolf-Watz, H. (2006) Protein delivery into eukaryotic cells by type III secretion machines. *Nature* **444,** 567–573

3. Marlovits, T. C., Kubori, T., Sukhan, A., Thomas, D. R., Galán, J. E., and Unger, V. M. (2004) Structural insights into the assembly of the type III secretion needle complex. *Science* **306,** 1040–1042

4. Mueller, C. A., Broz, P., and Cornelis, G. R. (2008) The type III secretion system tip complex and translocon. *Mol. Microbiol.* **68,** 1085–1095

5. Schraidt, O., and Marlovits, T. C. (2011) Three-dimensional model of *Salmonella*'s needle complex at subnanometer resolution. *Science* **331,** 1192–1195

6. Matteï, P.-J., Faudry, E., Job, V., Izoré, T., Attree, I., and Dessen, A. (2011) Membrane targeting and pore formation by the type III secretion system translocon. *FEBS J.* **278,** 414–426

7. Cornelis, G. R. (2002) The *Yersinia* Ysc-Yop "Type III" weaponry. *Nat. Rev. Mol. Cell Biol.* **3,** 742–752

8. Galán, J. E. (2001) *Salmonella* interactions with host cells: type III secretion at work. *Annu. Rev. Cell Dev. Biol.* **17,** 53–86

9. Moraes, T. F., Spreter, T., and Strynadka, N. C. (2008) Piecing together the type III injectisome of bacterial pathogens. *Curr. Opin. Struct. Biol.* **18,** 258–266

10. Frithz-Lindsten, E., Holmström, A., Jacobsson, L., Soltani, M., Olsson, J., Rosqvist, R., and Forsberg, A. (1998) Functional conservation of the effector protein translocators PopB/YopB and PopD/YopD of *Pseudomonas aeruginosa* and *Yersinia pseudotuberculosis. Mol. Microbiol.* **29,** 1155–1165

11. Goure, J., Pastor, A., Faudry, E., Chabert, J., Dessen, A., and Attree, I. (2004) The V antigen of *Pseudomonas aeruginosa* is required for assembly of the functional PopB/PopD translocation pore in host cell membranes. *Infect. Immun.* **72,** 4741–4750

12. Schoehn, G., Di Guilmi, A. M., Lemaire, D., Attree, I., Weissenhorn, W., and Dessen, A. (2003) Oligomerization of type III secretion proteins PopB and PopD precedes pore formation in *Pseudomonas. EMBO J.* **22,** 4957–4967

13. Faudry, E., Vernier, G., Neumann, E., Forge, V., and Attree, I. (2006) Synergistic pore formation by type III toxin translocators of *Pseudomonas aeruginosa. Biochemistry* **45,** 8117–8123

14. Romano, F. B., Rossi, K. C., Savva, C. G., Holzenburg, A., Clerico, E. M., and Heuck, A. P. (2011) Efficient isolation of *Pseudomonas aeruginosa* type III secretion translocators and assembly of heteromeric transmembrane pores in model membranes. *Biochemistry* **50,** 7117–7131

15. Kaufman, M. R., Jia, J., Zeng, L., Ha, U., Chow, M., and Jin, S. (2000) *Pseudomonas aeruginosa*-mediated apoptosis requires the ADP-ribosylating activity of ExoS. *Microbiology* **146,** 2531–2541

16. West, S. E., Romero, M. J., Regassa, L. B., Zielinski, N. A., and Welch, R. A. (1995) Construction of *Actinobacillus pleuropneumoniae-Escherichia coli* shuttle vectors: expression of antibiotic-resistance genes. *Gene* **160,** 81–86

17. Vallis, A. J., Finck-Barbançon, V., Yahr, T. L., and Frank, D. W. (1999) Biological effects of *Pseudomonas aeruginosa* type III-secreted proteins on CHO cells. *Infect. Immun.* **67,** 2040–2044

18. Gibson, D. G., Young, L., Chuang, R.-Y., Venter, J. C., Hutchison, C. A., 3rd, and Smith, H. O. (2009) Enzymatic assembly of DNA molecules up to several hundred kilobases. *Nat. Methods* **6,** 343–345

19. Ross, J. L., and Dixit, R. (2010) Multiple color single molecule TIRF imaging and tracking of MAPs and motors. *Methods Cell Biol.* **95,** 521–542

20. Díaz-Valencia, J. D., Morelli, M. M., Bailey, M., Zhang, D., Sharp, D. J., and Ross, J. L. (2011) *Drosophila* Katanin-60 depolymerizes and severs at microtubule defects. *Biophys. J.* **100,** 2440–2449

21. Yeow, E. K., and Clayton, A. H. (2007) Enumeration of oligomerization states of membrane proteins in living cells by homo-FRET spectroscopy: theory and application. *Biophys. J.* **92,** 3098–3104

22. Runnels, L. W., and Scarlata, S. F. (1995) Theory and application of fluorescence homotransfer to melittin oligomerization. *Biophys. J.* **69,** 1569–1583

23. Bergström, F., Mikhalyov, I., Hägglöf, P., Wortmann, R., Ny, T., and Johansson, L. B. (2002) Dimers of dipyrrometheneboron difluoride (BODIPY) with light spectroscopic applications in chemistry and biology. *J. Am. Chem. Soc.* **124,** 196–204

24. Mikhalyov, l., Gretskaya, N., Bergström, F., and Johansson, L. B.-Å. (2002) Electronic ground and excited state properties of dipyrrometheneboron difluoride (BODIPY): dimers with application to biosciences. *Phys. Chem. Chem. Phys.* **4,** 5663–5670

25. Song, X., and Swanson, B. I. (2001) Rapid assay for avidin and biotin based on fluorescence quenching. *Anal. Chim. Acta* **442,** 79–87

26. Zhuang, X., Ha, T., Kim, H. D., Centner, T., Labeit, S., and Chu, S. (2000) Fluorescence quenching: a tool for single-molecule protein-folding study. *Proc. Natl. Acad. Sci. U.S.A.* **97,** 14241–14244

27. Karolin, J., Johansson, L. B.-A., Strandberg, L., and Ny, T. (1994) Fluorescence and absorption spectroscopic properties of dipyrrometheneboron difluoride (BODIPY) derivatives in liquids, lipid membranes, and proteins. *J. Am. Chem. Soc.* **116,** 7801–7806

28. Rosconi, M. P., Zhao, G., and London, E. (2004) Analyzing topography of membrane-inserted diphtheria toxin T domain using BODIPY-streptavidin: at low pH, helices 8 and 9 form a transmembrane hairpin but helices 5–7 form stable nonclassical inserted segments on the cis side of the bilayer. *Biochemistry* **43,** 9127–9139

29. Kaya, S., Abe, K., Taniguchi, K., Yazawa, M., Katoh, T., Kikumoto, M., Oiwa, K., and Hayashi, Y. (2003) Oligomeric structure of P-type ATPases observed by single molecule detection technique. *Ann. N.Y. Acad. Sci.* **986,** 278–280

30. Groulx, N., McGuire, H., Laprade, R., Schwartz, J.-L., and Blunck, R. (2011) Single molecule fluorescence study of the *Bacillus thuringiensis* toxin Cry1Aa reveals tetramerization. *J. Biol. Chem.* **286,** 42274–42282

31. Tamm, L. K., and McConnell, H. M. (1985) Supported phospholipid bilayers. *Biophys. J.* **47,** 105–113

32. Gawrisch, K. (2005) The dynamics of membrane lipids. in *The Structure of Biological Membranes* (Yeagle, P. L., ed) 2nd Ed., pp. 147–171, CRC Press, Boca Raton, FL

33. Wagner, M. L., and Tamm, L. K. (2000) Tethered polymer-supported planar lipid bilayers for reconstitution of integral membrane proteins: silane-polyethyleneglycol-lipid as a cushion and covalent linker. *Biophys. J.* **79,** 1400–1414

34. Wang, Y., Malenbaum, S. E., Kachel, K., Zhan, H., Collier, R. J., and London, E. (1997) Identification of shallow and deep membrane-penetrating forms of diphtheria toxin T domain that are regulated by protein concentration and bilayer width. *J. Biol. Chem.* **272,** 25091–25098

35. Chenal, A., Savarin, P., Nizard, P., Guillain, F., Gillet, D., and Forge, V. (2002) Membrane protein insertion regulated by bringing electrostatic and hydrophobic interactions into play: a case study with the translocation domain of the diphtheria toxin. *J. Biol. Chem.* **277,** 43425–43432

36. Thuduppathy, G. R., Terrones, O., Craig, J. W., Basañez, G., and Hill, R. B. (2006) The N-terminal domain of Bcl-x_L reversibly binds membranes in a pH-dependent manner. *Biochemistry* **45,** 14533–14542

37. Vargas-Uribe, M., Rodnin, M. V., and Ladokhin, A. S. (2013) Comparison of membrane insertion pathways of the apoptotic regulator Bcl-xL and the diphtheria toxin translocation domain. *Biochemistry* **52,** 7901–7909

38. van der Goot, F. G., González-Mañas, J. M., Lakey, J. H., and Pattus, F. (1991) A "molten-globule" membrane-insertion intermediate of the pore-forming domain of colicin A. *Nature* **354,** 408–410

39. Faudry, E., Job, V., Dessen, A., Attree, I., and Forge, V. (2007) Type III secretion system translocator has a molten globule conformation both in its free and chaperone-bound forms. *FEBS J.* **274,** 3601–3610

40. Das, S. K., Darshi, M., Cheley, S., Wallace, M. I., and Bayley, H. (2007) Membrane protein stoichiometry determined from the step-wise photobleaching of dye-labelled subunits. *ChemBioChem* **8,** 994–999

41. Arant, R. J., and Ulbrich, M. H. (2014) Deciphering the subunit composition of multimeric proteins by counting photobleaching steps. *ChemPhysChem* **15,** 600–605

42. Montagner, C., Arquint, C., and Cornelis, G. R. (2011) Translocators YopB and YopD from *Yersinia enterocolitica* form a multimeric integral membrane complex in eukaryotic cell membranes. *J. Bacteriol.* **193,** 6923–6928

43. Goure, J., Broz, P., Attree, O., Cornelis, G. R., and Attree, I. (2005) Protec-

tive anti-V antibodies inhibit *Pseudomonas* and *Yersinia* translocon assembly within host membranes. *J. Infect. Dis.* **192,** 218–225

44. Picking, W. L., Nishioka, H., Hearn, P. D., Baxter, M. A., Harrington, A. T., Blocker, A., and Picking, W. D. (2005) IpaD of *Shigella flexneri* is independently required for regulation of Ipa protein secretion and efficient insertion of IpaB and IpaC into host membranes. *Infect. Immun.* **73,** 1432–1440

45. Hume, P. J., McGhie, E. J., Hayward, R. D., and Koronakis, V. (2003) The purified Shigella IpaB and Salmonella SipB translocators share biochemical properties and membrane topology. *Mol. Microbiol.* **49,** 425–439

46. Dickenson, N. E., Arizmendi, O., Patil, M. K., Toth, R. T., 4th, Middaugh, C. R., Picking, W. D., and Picking, W. L. (2013) N-terminus of IpaB provides a potential anchor to the Shigella type III secretion system tip complex protein IpaD. *Biochemistry* **52,** 8790–8799

47. Adam, P. R., Dickenson, N. E., Greenwood, J. C., 2nd, Picking, W. L., and Picking, W. D. (2014) Influence of oligomerization state on the structural properties of invasion plasmid antigen B from *Shigella flexneri* in the presence and absence of phospholipid membranes. *Proteins* **82,** 3013–3022

48. Veenendaal, A. K., Hodgkinson, J. L., Schwarzer, L., Stabat, D., Zenk, S. F., and Blocker, A. J. (2007) The type III secretion system needle tip complex mediates host cell sensing and translocon insertion. *Mol. Microbiol.* **63,** 1719–1730

49. Epler, C. R., Dickenson, N. E., Olive, A. J., Picking, W. L., and Picking, W. D. (2009) Liposomes recruit IpaC to the *Shigella flexneri* type III secretion apparatus needle as a final step in secretion induction. *Infect. Immun.* **77,** 2754–2761

50. Mueller, C. A., Broz, P., Müller, S. A., Ringler, P., Erne-Brand, F., Sorg, I., Kuhn, M., Engel, A., and Cornelis, G. R. (2005) The V-antigen of *Yersinia* forms a distinct structure at the tip of injectisome needles. *Science* **310,** 674–676

51. Chang, J., Myeni, S. K., Lin, T. L., Wu, C. C., Staiger, C. J., and Zhou, D. (2007) SipC multimerization promotes actin nucleation and contributes to *Salmonella*-induced inflammation. *Mol. Microbiol.* **66,** 1548–1556

52. Osiecki, J. C., Barker, J., Picking, W. L., Serfis, A. B., Berring, E., Shah, S., Harrington, A., and Picking, W. D. (2001) IpaC from *Shigella* and SipC from *Salmonella* possess similar biochemical properties but are functionally distinct. *Mol. Microbiol.* **42,** 469–481

53. Mounier, J., Popoff, M. R., Enninga, J., Frame, M. C., Sansonetti, P. J., and Van Nhieu, G. T. (2009) The IpaC carboxy terminal effector domain mediates Src-dependent actin polymerization during *Shigella* invasion of epithelial cells. *PLoS Pathog.* **5,** e1000271

54. Mounier, J., Boncompain, G., Senerovic, L., Lagache, T., Chrétien, F., Perez, F., Kolbe, M., Olivo-Marin, J.-C., Sansonetti, P. J., and Sauvonnet, N. (2012) *Shigella* effector IpaB-induced cholesterol relocation disrupts the Golgi complex and recycling network to inhibit host cell secretion. *Cell Host Microbe* **12,** 381–389

55. Senerovic, L., Tsunoda, S. P., Goosmann, C., Brinkmann, V., Zychlinsky, A., Meissner, F., and Kolbe, M. (2012) Spontaneous formation of IpaB ion channels in host cell membranes reveals how *Shigella* induces pyroptosis in macrophages. *Cell Death Dis.* **3,** e384

56. Cymer, F., von Heijne, G., and White, S. H. (2015) Mechanisms of integral membrane protein insertion and folding. *J. Mol. Biol.* **427,** 999–1022

57. Selkrig, J., Leyton, D. L., Webb, C. T., and Lithgow, T. (2014) Assembly of β-barrel proteins into bacterial outer membranes. *Biochim. Biophys. Acta* **1843,** 1542–1550

58. Dunstone, M. A., and Tweten, R. K. (2012) Packing a punch: the mechanism of pore formation by cholesterol dependent cytolysins and membrane attack complex/perforin-like proteins. *Curr. Opin. Struct. Biol.* **22,** 342–349

59. Gilbert, R. J., Dalla Serra, M., Froelich, C. J., Wallace, M. I., and Anderluh, G. (2014) Membrane pore formation at protein: lipid interfaces. *Trends Biochem. Sci.* **39,** 510–516

60. Johnson, B., and Heuck, A. (2014) Perfringolysin O Structure and mechanism of pore formation as a paradigm for cholesterol-dependent cytolysins. in *MACPF/CDC Proteins: Agents of Defence, Attack and Invasion* (Anderluh, G., and Gilbert, R., eds) pp. 63–81, Springer, Netherlands

61. Radics, J., Königsmaier, L., and Marlovits, T. C. (2014) Structure of a pathogenic type 3 secretion system in action. *Nat. Struct. Mol. Biol.* **21,** 82–87

62. Dey, S., Basu, A., and Datta, S. (2012) Characterization of molten globule PopB in absence and presence of its chaperone PcrH. *Protein J.* **31,** 401–416

Type 3 Secretion Translocators Spontaneously Assemble a Hexadecameric Transmembrane Complex

Fabian B. Romano, Yuzhou Tang, Kyle C. Rossi, Kathryn R. Monopoli, Jennifer L. Ross and Alejandro P. Heuck

Access the most updated version of this article at doi: 10.1074/jbc.M115.681031

Alerts:
- When this article is cited
- When a correction for this article is posted

Click here to choose from all of JBC's e-mail alerts

This article cites 60 references, 14 of which can be accessed free at
http://www.jbc.org/content/291/12/6304.full.html#ref-list-1